Dynamics of domain walls in ferrodistortive materials II. Applications to $Pb_5Ge_3O_{11}$- and SbSI-type ferroelectrics

J. F. Currie,* A. Blumen,† M. A. Collins,‡ and John Ross
Department of Chemistry, Massachusetts Institute of Technology, Cambridge, Massachusetts 02139
(Received 1 September 1978)

In this article we apply the theory developed in the previous publication to the uniaxial displacive ferroelectrics $Pb_5Ge_3O_{11}$ and SbSI. We show that the parameters of our model can be determined from available experimental data for these substances. The values obtained are physically reasonable. With *no adjustable parameters* we calculate for lead germanate the wave-number and temperature dependence of the low-temperature central peak, the density of domain walls, and the polarization switching. For SbSI we evaluate the temperature and pressure dependence of the low-temperature central peak. The theoretical results agree quantitatively with the experimental data. We predict the, as yet unmeasured, temperature-dependent wall diffusion coefficient in $Pb_5Ge_3O_{11}$ and the mobility of its domain walls in a field.

I. INTRODUCTION

In this article we compare the experimentally established dynamical properties of domain walls in uniaxial displacive ferroelectrics with the theoretical results of the previous article.[1] We analyze in detail the experimental results for two different prototypical substances, lead germanate ($Pb_5Ge_3O_{11}$) and antimony sulphoiodide (SbSI), and with the help of our theory, relate their macroscopic properties (domain-wall motion and polarization change) to the microscopic properties (as obtained from light and neutron scattering).

A ferrodistortive phase transition is accompanied by one mode becoming soft.[2–4] In the ferrodistortive regime the lattice displacement pattern is characterized by the appearance of macroscopically observable domains.[5] The same microscopic forces which produce the soft-phonon mode lead to such macroscopic features as thermal and dielectric anomalies, domain formation, domain-wall mobility and diffusion. These features are important factors in determining the optical and ferroelectric behavior of these materials. The macroscopic mobile domain structures are of practical interest as the active components in optical switching and memory devices.[6–8] It is the number of domains and their mobility which determines such crucial properties as switching time, effective polarization, hysteresis, and power dissipation.[9–11] Here we show that the parameters of the model in Ref. 1 can be determined from the established properties of ferroelectrics, with particular reference to the soft mode. These parameters are then used to calculate the scattering intensity, the transport coefficients of the domain walls, the wall-number density and polarization switching times. We compare these theoretical predictions with the available data on $Pb_5Ge_3O_{11}$ and SbSI.

In Sec. II we review the geometry of domains in uniaxial ferroelectrics. We discuss their nucleation and growth, and the mechanism by which domain walls propagate in applied fields. Section III summarizes the available experimental data for $Pb_5Ge_3O_{11}$ and SbSI. The experiments considered are in the main concerned with light, neutron, and x-ray scattering and with polarization and hysteresis effects. Section IV demonstrates how the model parameters of our theory can be determined from the light, neutron, and x-ray scattering data. We discuss the determined values of the seven model parameters for both substances and show that the values are physically reasonable. Using these fixed values, with *no adjustable parameters,* we calculate seven additional observable properties and compare the results with available data.

Our theory predicts a very narrow central peak in the light- and neutron-scattering spectrum below the critical temperature T_c, due to the Brownian motion of domain walls.

Since our theoretical results are only valid below T_c, where fluctuations are small, we do not attempt to describe the anomalous central peak observed near T_c. However, the results presented below clearly indicate that the Brownian motion of walls does *not* contribute significantly to the scattering near T_c, at least in the linear analysis employed in Ref. 1. Moreover, we calculate the wave-number and temperature dependence of the low-temperature peak in neutron scattering for $Pb_5Ge_3O_{11}$ and compare with the experimental findings. We also evaluate the pressure dependence of the central peak in light scattering for SbSI and compare it to the available data. All these

theoretical results agree well with the measurements. The number density of domain walls is determined from these data and is shown to be temperature independent. The wall number density obtained is in fair agreement with direct measurements on other samples. Furthermore, for $Pb_5Ge_3O_{11}$ we calculate the temperature dependence of the domain-wall diffusion coefficient, and of the wall velocity in an applied field, and find that they match the observed polarization switching times. These properties have not been calculated for SbSI due to a lack of available data.

II. PROPERTIES OF DOMAINS AND DOMAIN WALLS

Domain geometry and domain-wall dynamics in ferroelectric materials are topics receiving a great deal of attention in the applied-physics literature.[9–14]

There is an abundance of experimental data and we focus on certain general characteristics of domains and domain walls in uniaxial materials. In this section we review the macroscopic properties of these substances relevant to our phenomenological model.

Above the transition temperature T_c a ferroelectric substance is in a phase of no polarization. Below T_c, the crystal undergoes a spontaneous symmetry breaking in which the equilibrium atomic positions shift to produce a new structure with a dipole moment in each unit cell. In uniaxial ferroelectrics the polarization $\vec{P}$ lies parallel to a unique crystallographic axis, say $\hat{z}$.[2] The free energy of domains with polarization $\pm\vec{P}$ is the same in the absence of an external field, $\vec{E}$. Generally, the crystal is divided into regions or domains of opposite polarization with the "up" domains separated from the "down" domains by domain walls. The actual domain structure and geometry in a particular crystal in equilibrium is determined by the condition that the total free energy of the sample be a minimum. However, the domain structure in a given crystal depends crucially on the preparation and history of that crystal; the sample has a particular domain configuration corresponding to a long-lived metastable state, and it is this nonequilibrium configuration which is probed in a given experiment.

On the basis of macroscopic arguments[5] pertaining to equilibrium, the polarization cannot vary along the ferroelectric axis: domain walls must be parallel to this axis, since the component of the electric displacement field $\vec{D}$ normal to the wall must be continuous. For the same reason states with domain walls perpendicular to $\hat{z}$ are short lived. Such states can be created by frequent switching of high electric fields, if the samples are large in the $\hat{z}$ direction.[12] In thin crystals the domains are cylindrical parallel to $\hat{z}$,[10] and their position is fully determined by a two-dimensional projection (see Fig. 1).

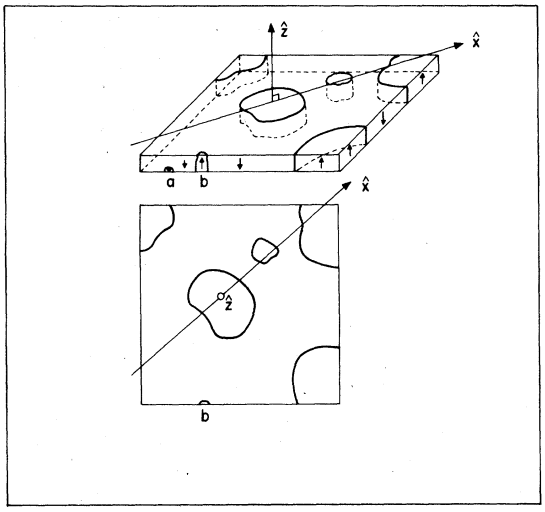

FIG. 1. Schematic representation of domains in a uniaxial ferroelectric crystal. A section of the crystal is shown in perspective and in projection showing the plane perpendicular to $\hat{z}$. The small volume labeled a represents a nucleus of one phase in the other. The segment labeled b denotes this nucleus after a period of rapid growth in the $\hat{z}$ direction. Larger domains, evident after a period of lateral growth in an applied field, are also shown. The axis $\hat{x}$ denotes an arbitrary direction in the plane perpendicular to $\hat{z}$.

By applying sufficiently large electric fields in the $\hat{z}$ direction (larger than the coercive field E_c) one can produce a monodomain crystal. On removing the applied field the polarization of the sample decreases to a value near P_s,[15] the spontaneous polarization. Application of an opposite field causes the crystal to reverse its polarization.

Observations of this process reveal that polarization reversal is a heterogeneous, nucleation and growth phenomenon.[9–11] Initially a number of nuclei, determined by sample preparation, form [see the nucleus of reversed polarization labeled (a) in Fig. 1]. These nuclei grow rapidly in the $\hat{z}$ direction to form cylindrical domains [see the domain labeled (b) in Fig. 1]. The domains are circular, so as to minimize the surface tension. Subsequent growth occurs laterally, and when the domains reach macroscopic size, the wall motion corresponds to translation of planes normal to z through the crystal.

Any experiment which probes the local structure of domains in a plane perpendicular to $\hat{z}$ along a particular axis $\hat{x}$ sees many planes of domain walls oriented at different angles (see Fig. 1). For a random distribution of *circular* domains the average apparent domain-wall width d_a is related to d, the width normal to the surface by

$$d_a = \tfrac{1}{2}\pi d \quad . \tag{2.1}$$

Also the average apparent wall velocity v_a is

$$v_a = \tfrac{1}{2}\pi v \ , \tag{2.2}$$

where v is the radial velocity. If the real domain structure is not exactly circular, then the factor multiplying d and v changes slightly.

Another manifestation of domains in polarization-switching experiments is that of the Barkhausen pulses. These are due to abrupt changes in polarization, mostly ascribed to the formation and annihilation of whole domains.[14]

The lateral growth of domains most likely does not occur as a completely coherent process, but rather by polarization reversal in individual chains along the $\hat{z}$ axis. Each chain switches as a result of large fluctuations of opposite polarization expanding rapidly along the $\hat{z}$ direction.[12] This multistep mechanism lowers considerably the barrier against lateral domain-wall motion.

Domain formation, nucleation and growth are ubiquitous phenomena in ferroelectrics. However, in the absence of an electric field large energies are required to form domains (except near T_c). Thus at lower temperatures domain walls are neither created nor destroyed thermally. Changes in temperature below T_c do not affect the density of domain walls[16,17] (see also Sec. IV). One is thus forced to treat the crystal as a metastable system rather than one in true equilibrium.

III. PROPERTIES OF $Pb_5Ge_3O_{11}$ AND SbSI

In this section we present the properties of two representative ferroelectrics of particular recent interest, lead germanate ($Pb_5Ge_3O_{11}$) and antimony sulphoiodide (SbSI), and use them in the next section to test our model. We choose these substances because they are both uniaxial and displacive,[18,19] as required by our theory. However, these materials differ in other important respects. SbSI is filamentary[20] and has a pronounced first-order phase transition, whereas $Pb_5Ge_3O_{11}$ is more isotropic and its discontinuity, at T_c, in the spontaneous polarization is smaller.

Lead germanate, $Pb_5Ge_3O_{11}$, is a uniaxial ferroelectric which shows a first-order phase transition at $T_c = 451$ K and standard pressure.[21,22] X-ray[18,23] and neutron[24] studies reveal a chain-like structure in the $\hat{z}$ direction with single and double germanate tetrahedra alternately disposed with axes of symmetry parallel to $\hat{z}$, and lead atoms forming a layer structure of regular spacing perpendicular to $\hat{z}$. Large single crystals of lead germanate may be grown so that good samples of different orientation are readily available for studies of scattering or domain-wall mobility.

Above T_c the crystal is paraelectric with $C_{3h}^1(P\bar{6})$ hexagonal symmetry and lattice constants $a = 10.26$ Å and $c = 10.69$ Å.[18] Below T_c the crystal is ferroelectric with trigonal symmetry C_3^1 ($P3$), and axis of polarization parallel to $\hat{z}$; the crystal looses a mirror symmetry normal to the $\hat{z}$ axis.[23] The static dielectric constant ϵ_{33} is observed to have an anomaly at T_c and to obey a Curie-Weiss law in its temperature dependence above and below T_c.[25] Raman experiments[26] show a mode that softens.

X-ray and neutron work has also provided information on the movements of the equilibrium positions of the atoms in the unit cell.[18,23] Transforming from the paraelectric phase involves small torsions of the germanate tetrahedra and shifts of the lead atoms. The largest movement at 293 K of an oxygen atom is 0.36 Å along the $\hat{z}$ axis and nearly as much in the plane normal to $\hat{z}$, while the largest lead and germanium displacements are about 0.15 Å along the $\hat{z}$ axis. All displacements are less than 5% of the lattice constants. These experiments also confirm that the transition is displacive.[18]

Lead germanate can be used in ceramic form for high-capacitance condensers or in crystalline form in transducers, where use is made of its piezeoelectric behavior. It is employed in optical memory devices because it shows pronounced hysteresis and optical activity[8]; lead germanate has fast switching times t_s in the microsecond range and needs a relatively weak coercive field E_c ($\lesssim$14kV/cm at 50 Hz).[12]

Antimony sulphoiodide SbSI, is a ferroelectric belonging to the V-VI-VII class of semiconductors in which one element in each of the series V (Sb,Bi), VI (S,Se), and VII (Cl,Br,I) appears. It is quite difficult to grow single crystals of these materials[20]; the ternary system is unstable with respect to phase separation.[14] In addition to being ferroelectric these compounds are photoconductors and highly piezoelectric.[27] X-ray and neutron structure studies[19,28–30] show that SbSI is filamentary in structure with the filaments parallel to $\hat{z}$. The crystal symmetry is orthorhomic D_{2h}^{16} ($Pnam$) above T_c (293 K) and orthorhombic C_{2v}^9 ($Pna2_1$) below T_c. The atomic shifts at 274 K are parallel to $\hat{z}$ with Sb moving 0.2 Å, S moving 0.02 Å, and I remaining fixed.[30] There is no appreciable movement of the atoms normal to $\hat{z}$. Polarization studies reveal switching times in the microsecond range for coercive fields of 1 kV/cm.[31]

We note that both these substances obey the Curie-Weiss law above T_c,[25,31]

$$\epsilon_{33}^{-1} \propto T - T_B, \quad T_B < T_c \ , \tag{3.1}$$

and that the soft-mode frequency $\omega_0(T)$ closely follows the form[26,32]

$$\omega_0^2(T)/\omega_0^2(0) = (T_A - T)/T_A, \quad T_A > T_c \tag{3.2}$$

below T_c. We can fit Eq. (3.2) to the observed soft-mode frequencies of both substances to within 6%.

TABLE I. A summary of the experimentally determined properties of $Pb_5Ge_3O_{11}$ and SbSI with reference to the source used. The symbols $c_{\parallel}$ and $c_{\perp}$ denote the acoustic velocity parallel and perpendicular to the $\hat{z}$ (ferroelectric) axis, respectively. The neutron spectrometer frequency resolution in experiments on SbSI (Ref. 37) has not been given and is taken to be the same as Ref. 16.

	Observed property (at 1 atm)	$Pb_5Ge_3O_{11}$	Ref.	SbSI	Ref.
No.	Order of phase transition	first		first	
	Transition temperature, T_c (K)	451	22	293	28–30
	Paraelectric phase				
	Structure	$C_{3h}^1(P\bar{6})$		$D_{2h}^{16}(Pnam)$	
	Lattice constants (Å) a	10.26		18.50	
	b	10.26 at 473 K	18	10.14 at 300 K	37
	c	10.69		4.09	
	Ferroelectric phase				
	Structure	$C_3^1(P3)$	23	$C_{2v}^9(Pna2_1)$	19,37
MI	Lattice constants (Å) a	10.25		18.51	
	b	10.25 at 293 K	23	10.13 at 280 K	37
	c	10.69		4.11	
	Formula units in unit cell	3		4	
MII	Soft-mode half-width γ (cm^{-1})	14 at 293 K	26	11 at 284 K	38
MIII	Acoustic velocities				
	$\parallel\hat{z}, c_{\parallel}$ ($cm\,sec^{-1}$)	3.15×10^5	36	3.0×10^5	37,39
	$\perp\hat{z}$, $c_{\perp}$ ($cm\,sec^{-1}$)	2.60×10^5		2.4×10^5	
MIV	Neutron Spectrometer Resolution (cm^{-1})	0.88	16	(0.88)	
MV	Soft-mode frequency $\omega_0(T)=\omega_0(0)(1-T/T_A)^{1/2}$				
	$\omega_0(0)$ (cm^{-1}) [extrapolation]	51	26	57	32,33,3
	T_A (K) [extrapolation]	500 ± 20	26	435 ± 15	32
MVI	Maximum ionic displacement $u_0(T)$ (Å)	0.36 at 293 K	18	0.2 at 278 K	30
MVII	Spontaneous Polarization $P_s(T)$ ($\mu C\ cm^{-2}$) at 50 Hz	4.6 at 300 K	22,12,25	20 at 273 K	31
	Mass per unit cell m_u (proton mass units)	4.29×10^3		1.12×10^3	
	Curie-Weiss temperature T_B (K)	447	25	283	31
	Coercive Field $E_C(T)$ ($kV\,cm^{-1}$) at 50 Hz	14 at 293 K	25,12,22	0.1 at 273 K	31
	Tricritical Pressure $p_t(T)$ (kbar)	···	···	1.4 at 235 K	33

We recall that for a second-order phase transition, one has $T_A = T_B = T_c$. Light- and neutron-scattering experiments reveal a prominent central-peak feature well below T_c,[16,33] in addition to an anomalous central peak near the critical temperature.[16,34,35] The low-temperature central peak has been attributed to the presence of domain walls[16] though its origin and form have not been properly explained. This peak has a width Γ which is below current experimental resolution (which we denote by $\Delta\omega$).

The data for important measured properties of the two substances are summarized in Table I. In Sec. IV we use these data to determine the parameters of our model.

IV. APPLICATION OF THE MODEL TO $Pb_5Ge_3O_{11}$ AND SbSI

This section shows how the simple one-dimensional model of the previous publication[1] can be applied to the two chosen prototype crystals.

In our model the soft-mode displacement is the same for all equivalent atoms within each plane normal to $\hat{x}$. We characterize this displacement by a single function $u(x,t)$ which describes the displacement pattern for the different planes. The equation of motion for $u(x,t)$ is[1]

$$m\frac{\partial^2 u}{\partial t^2}+m\lambda\frac{\partial u}{\partial t}+Au+Bu^3-mc_0^2\frac{\partial^2 u}{\partial x^2}=R(x,t)+e^*E \tag{4.1}$$

in the displacive limit. Here E is an applied (electric) field and $R(x,t)$ is the random fluctuating force as defined in Eqs. (2.9)–(2.11) of Ref. 1. Equation (4.1) contains seven parameters: (i) l, the unit cell length along the $\hat{x}$ axis [a parameter of $R(x,t)$]; (ii) $\lambda(T,p)$, the damping of the displacement pattern motion; (iii) c_0, the harmonic coupling coefficient resulting from strain and electrostatic forces; (iv) m, the effective mass of the atoms whose motion in each plane is correlated; (v) $A(T,p)$, the crystalline-field quadratic coefficient which varies strongly with temperature and pressure; (vi) B, the crystalline-field quartic coefficient (temperature independent); (vii) e^*, the effective charge of the atoms whose motion in each plane is correlated.

We fix these parameters using the published data on the following seven independent measurements: (I) a,b,c, the crystalline-lattice constants; (II) $\gamma(T,p)$, the damping determined from the soft-mode lineshape; (III) $c_\perp$, the acoustic velocity normal to the $\hat{z}$ axis; (IV) $\Gamma(k,T,p)$, the half width of the central peak; k is the wave number; (V) $\omega_0(0,T,p)$, the frequency of the soft mode at zero wave number; (VI) the temperature- and pressure-dependent average atomic positions; (VII) $P_s(T,p;E,\nu)$, the spontaneous polarization for a given field strength E cycled at frequency ν. The detailed procedure whereby parameters (i) through (vii) are fixed by measurements, hereafter referred to as M(I)–M(VII) is as follows: (i) l is determined from a,b,c according to the particular $\hat{x}$ axis probed in a given experiment. (ii) From Eq. (5.14) of Ref. 1 we identify λ with γ M(II); (iii) The conclusive assignment of c_0 for $Pb_5Ge_3O_{11}$ and SbSI from the soft-mode dispersion relation, $[\omega_0^2(k)=\omega_0^2(0)+c_0^2k^2$, see Eq. (5.8) of Ref. 1] is difficult due to the paucity of experimental data. A rough estimate of c_0 is taken to be $c_\perp$ M(III).

We determine the remaining parameters (iv) through (vii) from M(IV)–(VII) as follows: (iv) The mass m is obtained from the domain wall diffusion coefficient D, which is in turn given by the frequency width Γ M(IV) of the central peak in the neutron scattering data. We have [see Eq. (5.16) of Ref. 1],

$$D(T)=\Gamma(k,T)/k^2 \tag{4.2}$$

and [see Eq. (4.13), (2.7), and (5.8) of Ref. 1]

$$m=\frac{k_BT}{D(T)\lambda(T)}\left[\frac{3c_0l}{2u_0^2(T)\omega_0(0,T)}\right]. \tag{4.3}$$

Here ω_0 is the observed soft-mode frequency M(V) and $u_0(T)$ is estimated to be the largest observed atomic displacement in the unit cell, M(VI). For both $Pb_5Ge_3O_{11}$ and SbSI, the central-peak width is below experimental resolution $\Delta\omega$, even at the Brillouin-zone boundary, where Γ is largest. Thus, we can only given an upper bound for D as

$$D(T_1)\leq\frac{\Delta\omega l^2}{2\pi^2}. \tag{4.4}$$

Since $D(T)$ increases with temperature,[1] a best upper bound is obtained by taking in Eq. (4.4) the highest temperature T_1 ($T_1<T_c$) at which the central peak can be unambiguously identified. Thus, the value of m given by Eq. (4.3) is a lower bound. (v) $A(T)$ is found from the light scattering data on the soft-mode frequency M(V) [see Eq. (5.8) of Ref. 1] and the above value for m (iv)

$$|A(T)|=\tfrac{1}{2}m\omega_0^2(0,T). \tag{4.5}$$

(vi) B is obtained from the displacement $u_0(T)$ M(VI) by [see Eq. (3.13) of Ref. 1]

$$B=\frac{|A(T)|}{u_0^2(T)} \tag{4.6}$$

and is temperature independent. (vii) The effective charge e^* is obtained combining the results from experiments M(IV)–(VII) as follows. A charge e is associated with the displacement in each unit cell and gives rise to the observed spontaneous polarization P_s M(VII) so that we have

$$e=V_uP_s(T)/u_0(T), \tag{4.7}$$

where V_u is the unit cell volume determined from M(I). The effective charge of the particle of mass m (iv) is then given by

$$e^*=(m/m_u)e, \tag{4.8}$$

where m_u is the mass in the unit cell. The ratio m/m_u is a measure of the number of unit cells whose

TABLE II. The seven model parameters, and the domain-wall diffusion coefficient $D(T_1 = 350\ \text{K})$ determined for $Pb_5Ge_3O_{11}$ and SbSI. The large uncertainty in the value of u_0 M(VI) for SbSI produces considerable uncertainty in the parameters (iv) to (vii) for SbSI. These quantities are marked by parentheses.

No.	Determined Model Parameters	$Pb_5Ge_3O_{11}$	Derivation	SbSI
i	Unit-cell length along a axis (Å)	10.3	M(I)	18.5
ii	Damping parameter $\lambda(T)$ (cm^{-1})	14 at 293 K	M(II)	11 at 284 K
iii	Coupling constant c_0 ($cm\,sec^{-1}$)	2.6×10^5	M(III)	2.4×10^5
	Diffusion constant $D(T_1)$ ($cm^2\,sec^{-1}$)	8.9×10^{-5}	(4.4)	2.9×10^{-4}
iv	Effective mass m (proton mass units)	6.5×10^4	(4.3)	(1.0×10^5)
v	Crystalline-field quandratic coefficient $A(T)$ ($erg\,cm^{-2}$)	$1.0 \times (500 - T) \times 10^4$+	(4.5)	$(2.2 \times (435 - T) \times 10^4)$
vi	Crystalline-field quartic coefficient B ($erg\,cm^{-4}$)	1.6×10^{23}	(4.6)	(8.8×10^{23})
vii	Effective charge e^* (electron-charge units)	147	(4.8)	(4320)

motion is correlated in the plane.

This completes the determination of the model parameters. Their values for the two substances studied are reported in Table II. The values obtained for the parameters are generally quite reasonable and consistent with our model of a coherent motion of a group of atoms in the plane perpendicular to $\hat{x}$. We note that the determination of the parameters in SbSI is more uncertain due to the considerable uncertainty in the crystallographic results for the atomic displacement M(VI). The two studies reported[19,30] disagree by a factor of 2 in the largest observed displacement. We have used the larger value,[30] though even this result is associated with a calculated spontaneous polarization[30] which is a factor of two *below* the observed value. Thus, even the larger value[30] of the two reported appears to be abnormally small. We note that the effective mass obtained for $Pb_5Ge_3O_{11}$ is of the order of that of fifteen unit cells while for SbSI we find a considerably larger value. This implies a correlated motion of unit cells in the plane for $Pb_5Ge_3O_{11}$. This "correlation area" agrees well with the correlation length along $\hat{x}$ (derived below to be between two and three unit-cell lengths), considering that the coupling between cells in the $\hat{z}$ direction is stronger. A somewhat larger correlation area for SbSI is also expected on the basis of the strong coupling along $\hat{z}$ associated with the filamentary structure of the crystal (leading to a larger correlation length parallel to $\hat{z}$ than in lead germanate). The very reasonable value obtained for m suggests that the measured upper bound on $D(T_1)$ for $Pb_5Ge_3O_{11}$ is a good estimate for the wall diffusion coefficient. The unit cell charge e was determined at three temperatures for $Pb_5Ge_3O_{11}$ and is around ten electron charges and almost temperature independent (see Table III). This value for e is quite appropriate to a unit cell containing three formula units of $Pb_5Ge_3O_{11}$, and so indicates that the estimate of u_0 is accurate. The observed constancy of e confirms that the temperature dependence of $P_s(T)$ and $u_0(T)$ is the same [see Eq. (4.7)].

Having determined all seven parameters and shown that they have reasonable values we now proceed to calculate seven additional observable quantities using *no adjustable parameters.* We compute (viii) the wave number and temperature dependence of the quasi-elastic central peak in $Pb_5Ge_3O_{11}$, (ix) the pressure dependence of this peak in SbSI, (x) the temperature dependence of the domain wall width, (xi) the number density of domain walls n_w, (xii) the polarization switching time t_s, (xiii) the temperature dependence of the wall diffusion coefficient, and (xiv) the temperature dependence of the wall mobility μ. Of these, (viii)–(xii) have been measured and thus give five independent tests of the theory. The last two quantities have not yet been investigated empirically so our computed results remain as predictions. Properties (xi) and (xii) are not calculated for SbSI since there is no available data on both the low-temperature central peak and the soft phonon mode at the same temperature. Properties (xiii) and (xiv) have not been evaluated for SbSI since the temperature dependence of the soft-mode damping $\gamma(T)$ M(II) is not available for a range of temperatures below T_c.

Let us first consider in detail the wave number, temperature and pressure dependence of the central peak observed in scattering experiments. In the neutron scattering study of a sample of $Pb_5Ge_3O_{11}$

TABLE III. Derived quantities for $Pb_5Ge_3O_{11}$, using the parameters of Table II and the equations referenced. The domain-wall density n_w was obtained from Eq. (4.13) using Fig. 1 of Ref. 16 at 435 K [where the wave number $k = 0.05\ (2)^{1/2}\pi/l = 2.16 \times 10^6\ \text{cm}^{-1}$], and the parameters in Table II. The polarization switching time was obtained using n_w and v (350) given above.

Quantity	Value	Derivation
effective domain-wall mass $m^*(350)$ (proton mass units)	82	(4.13) of Ref. 1
number density of domain walls n_w (cm^{-1})	1.6×10^3	(4.13)
average domain length (micron)	5.9	n_w^{-1}
domain-wall mobility $\mu(350)$ (sec g^{-1})	1.1×10^8	(4.17)
domain-wall terminal velocity $v(350)$ (cm sec^{-1})	360	(4.17) [$E = 14$ kV/cm]
polarization switching times (μsec)	1.6	(4.20)

without deposited electrodes, three distinct scattering features are resolved: a soft phonon mode, a low-temperature quasielastic central peak, and an anomalous central peak whose amplitude is maximal near T_c and which rapidly attenuates above and below T_c.[16] We recall that our theory describes the low-temperature central peak as opposed to the anomalous feature near T_c. The former peak is very narrow [$\Gamma(k) < \Delta\omega$], has an amplitude linear in T and practically disappears on application of a large external field of 1 kV/cm, which eliminates most of the domain walls. This peak was assigned to scattering from domain walls.[16] We used the data of Ref. 16 to obtain the diffusion coefficient given in Table III.

In our model the integrated intensity of this central peak is given by [Eqs. (5.18) of Ref. 1]

$$I_3(k,T) = n_w \left[\frac{u_0 \pi}{\alpha} \operatorname{csch}\left(\frac{\pi k}{2\alpha} \right) \right]^2 , \tag{4.9}$$

$$= 4 n_w \frac{u_0^2}{k^2} , \quad \text{for small } k , \tag{4.10}$$

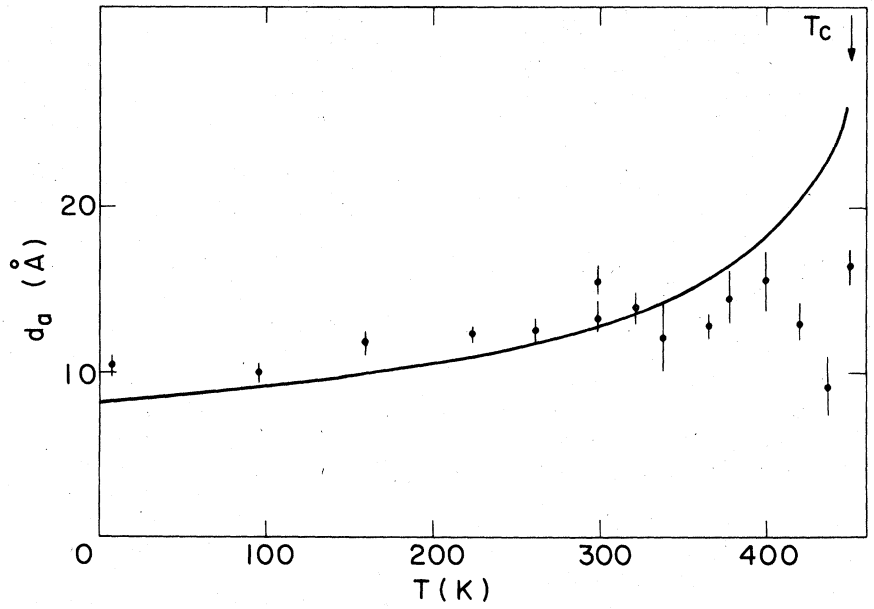

FIG. 2. Apparent domain-wall width d_a vs the crystal temperature T, for $Pb_5Ge_3O_{11}$. The solid line is the theoretical result of Eq. (4.12), the points are the experimental results of Ref. 16. The theoretical curve is not expected to be valid near T_c. The experimental points contain contributions from the anomalous central peak above 400 K.

where

$$\alpha(t) \equiv \tfrac{1}{2}\omega_0(0,T)/c_0 \tag{4.11}$$

is the inverse width of a planar domain wall [Eqs. (2.7) and (5.8) of Ref. 1]. As seen in Fig. 3 of Ref. 16, the functional form (4.9) provides a good fit to the k dependence of the observed central-peak intensity below T_c where the anomalous feature does not contribute to the scattering. From Eqs. (4.11) and (2.1) we have

$$d_a(t) = \tfrac{1}{2}\pi\alpha^{-1}(t) \ . \tag{4.12}$$

In Fig. 2 we compare $d_a(T)$ from Eq. (4.12) with the experimental results.[16] The quantitative agreement is very good up to 400 K. (We do not expect our model to be valid close to T_c and the presence of the anomalous central peak also obscures comparison beyond 400 K.) This agreement implies that our estimate for c_o is accurate and that the temperature dependence of $\alpha(T)$ is due to $\omega_0(0,T)$. Also, the value of $d_a(T)$ corresponds to a correlation length of two to three units cells along the $\hat{x}$ axis.

The absolute intensity of the central peak is proportional to the density of domain walls n_w [see Eq. (4.9)]; n_w depends crucially on preparation and varies from sample to sample. However, an estimate of the density n_w can be obtained from the ratio of the central- and phonon-peak integrated intensities I_3 and I_1, respectively. We have [Eq. (5.18) of Ref. 1]

$$n_w = \frac{\lambda D(T) k^2}{6\omega_0(T) c_0} \frac{I_3(T)}{I_1(T)} \ . \tag{4.13}$$

In $Pb_5Ge_3O_{11}$ the intensities of both the central and the phonon peaks have been reported at 435 K.[16] This allows us to normalize the reported central-peak intensity $I_3(T)$ to the phonon intensity $I_1(T)$. Using this data and Eq. (4.13) the domain-wall density reported in Table III at 350 K (where there is no contribution from the anomalous central peak) was obtained. The determined n_w corresponds to an average domain length of the order of six microns, which is in reasonable agreement with the domain lengths observed microscopically in other samples.[12]

In our model n_w is temperature independent. Using the calculated value of n_w at 350 K we calculate the temperature-dependence of $I_3(k,T)$ at fixed k from Eq. (4.9). In Fig. 3, I_3 is compared with the data reported in Ref. 16, normalized to the arbitrary intensity scale at 350 K. The agreement is excellent outside the narrow temperature range where the anomalous central peak appears. The small

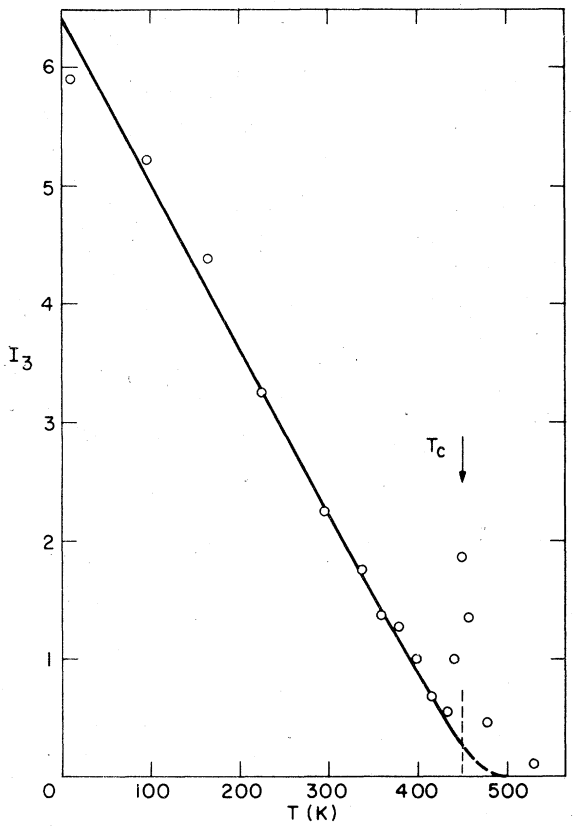

FIG. 3. Integrated intensity of the central peak in the neutron scattering from $Pb_5Ge_3O_{11}$ at fixed wave number ($k = 2.6 \times 10^6$ cm^{-1}) vs the crystal temperature T. The open circles are the experimental values presented in Fig. 2 of Ref. 16. The theoretical curve (solid line) was calculated from Eq. (4.9) using the values given in Table II and normalized to the arbitrary intensity scale of Ref. 16 at $T = 350$. The anomalous central peak, not considered by our model, is evident in the experimental results near T_c.

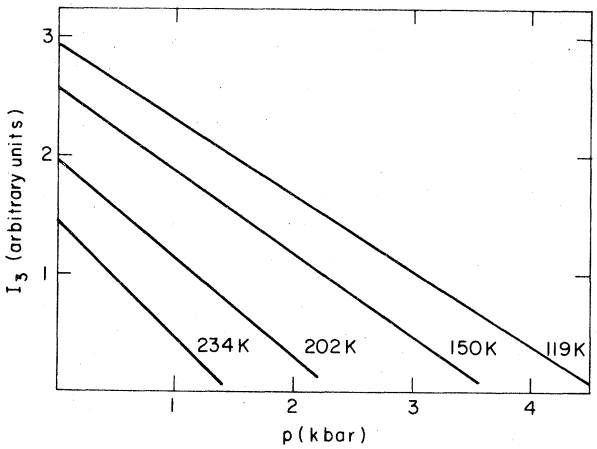

FIG. 4. The calculated intensity of the central peak in light scattering from SbSI in arbitrary units vs pressure at four crystal temperatures. The experimental results of Ref. 33, over a much more restricted pressure range, verify that $I_3(p)$ at 234 K is linear and extrapolates to zero at the same pressure as shown here.

discrepancy between the predicted and observed values may be described by a temperature dependence of n_w. Table IV presents $n_w(T)$ given by

$$n_w(T) = \frac{I_3(T)}{I_{\text{obs}}(T)} n_w(350) \quad . \tag{4.14}$$

The very small, essentially random, variations of n_w obtained lie well within the expected experimental error. This verifies the temperature independence of the domain-wall density.

In SbSI the pressure- and temperature-dependent soft-mode and central-peak intensity are known from Raman scattering experiments.[33] From Eqs. (4.5), (4.6), and (4.10) it follows that the central-peak intensity is proportional to $\omega_0^2(p,T)$. In Fig. 4 we predict $I_3(p)$ at four temperatures using the reported $\omega_0^2(p,T)$ data.[33] Figure 4 of Ref. 33 confirms the prediction for $I_3(p)$ at $T=234$ K; $I_3(p)$ is linear in p and extrapolates to zero at a pressure of 1.45 kbar.

Altogether, these results support the assignment of the low-temperature central peak to the Brownian motion of metastable domain walls. Equation (4.9) correctly describes the k dependence of this peak. The relation between the wall width $\alpha^{-1}(T)$, the soft mode frequency and c_0 is correctly given by Eq. (4.11). Moreover, the temperature and pressure dependence of the central-peak intensity is well reproduced assuming a constant density of domain walls. This supports our view that domain walls are not readily created thermally. The average domain length obtained is appropriate (Table III).

The macroscopic motion of the domain walls is described by the diffusion coefficient $D(T)$ and the mobility $\mu(T)$. The temperature dependence of $D(T)$ in $Pb_5Ge_3O_{11}$ was calculated using empirical values for $\lambda(T)$. From Eq. (4.3) we have

TABLE IV. The domain-wall density n_w, obtained from Fig. 2 and Eq. (4.14) is presented at several temperatures. The small variation of n_w is within the experimental accuracy of the observed central-peak intensity and the experimental data used to obtain the theoretical intensity. The charge per unit cell e was obtained from the temperature dependent spontaneous polarization reported in Ref. 22 using Eq. (4.17). The change in e over this temperature range is small in comparison with the change in P_s.

T (K)	$Pb_5Ge_3O_{11}$	
	n_w (cm^{-1})	e (electron-charge units)
0	1.5×10^3	...
100	1.7×10^3	...
200	1.7×10^3	...
300	1.6×10^3	9.3
350	1.6×10^3	9.5
400	1.8×10^3	10.0

$$D(T)/D(T_1) = \frac{T\lambda(T_1)u_o^2(T_1)\omega_0(0,T_1)}{T_1\lambda(T)u_0^2(T)\omega_0(0,T)} \quad . \tag{4.15}$$

Figure 5 presents $D(T)/D(350)$ calculated for $Pb_5Ge_3O_{11}$ from Eq. (4.15) using $\lambda(T)$ from Ref. 26. The significant increase in $\lambda(T)$ as $T\rightarrow T_c$ results in only a moderate increase in $D(T)$ with temperature. We are unaware of measurements of the wall-diffusion coefficient in these materials. However, a related quantity, the wall velocity in an applied field is readily measurable and was determined for some ferroelectrics. The velocity $v(T,E)$ in an external field is related to $D(T)$ by Eqs. (3.10) and (4.18) of Ref. 1, i.e.,

$$v(T,E) = \mu(T)e^*E \quad , \tag{4.16}$$

$$= \frac{2u_0(T)D(T)}{lk_BT}e^*E \quad , \tag{4.17}$$

where $\mu(T)$ is the mobility. Thus, the temperature

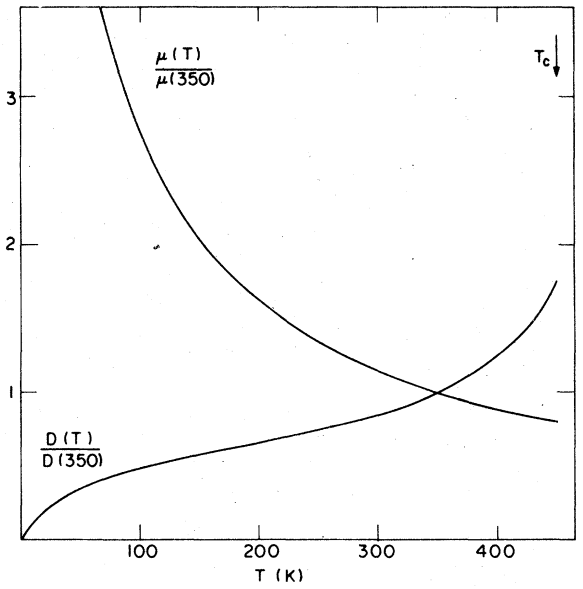

FIG. 5. The calculated temperature dependence of the domain-wall diffusion coefficient, $D(T)/D(350)$, [Eq. (4.15)] and mobility, $\mu(T)/\mu(350)$, [Eqs. (4.18) and (4.19)] for $Pb_5Ge_3O_{11}$. The calculations were performed using a damping $\lambda(T)$ fitted to the experimental data of Ref. 26: $\lambda(T)=(7.87T+331)(500-T)^{-1}$ cm^{-1}. Values for the other quantities required in Eqs. (4.15) and (4.19) were obtained from Table II. The values for $D(350)$ and $\mu(350)$ are given in Table III. We note that the temperature dependence of the wall velocity in a field, $v(T)/v(350)$, is the same as $\mu(T)/\mu(350)$ [Eq. (4.18)].

dependence of $v(T)$ is given by

$$v(T)/v(T_1) = \mu(T)/\mu(T_1) \quad , \tag{4.18}$$

$$= \frac{T_1 u_0(T) D(T)}{T u_0(T_1) D(T_1)} \quad . \tag{4.19}$$

The calculated velocity v for $Pb_5Ge_3O_{11}$ at 350 K in a field of 14 kV/cm is reported in Table III while $\mu(T)/\mu(350)$ is shown in Fig. 5. Thus $v(T)$ declines with increasing temperature, since the damping coefficient λ increases. Although for $Pb_5Ge_3O_{11}$ no direct measurements of the wall velocity normal to $\hat{z}$ have been reported, we can obtain a crude estimate of the accuracy of $v(T)$ as follows: The polarization switching time t is the time necessary to reverse 95% of the polarization of the sample.[10] As outlined in Sec. II, the final stage in the reversal of the crystal polarization involves the lateral growth of domains. Let us start with a completely polarized sample: The growth of nuclei in the $\hat{z}$ direction is a rapid process, if in addition nucleation of domains is rapid, then the lateral growth is the rate determining step for T_s. We can obtain a crude estimate of t_s as

$$t_s \sim (n_w v)^{-1} \quad . \tag{4.20}$$

Using the value of n_w given in Table III we obtain a switching time in the μsec range. This agrees quite well with typical switching times in fields of the order of 10 kV/cm. Thus, the wall velocity $v(T)$ that we report has the correct magnitude.

ACKNOWLEDGMENTS

The authors are grateful to Professor Robert Silbey and Professor J. W. Cahn for valuable discussions during the course of this work. This study was supported in part by the National Science Foundation and the Air Force Office for Scientific Research. J.F.C. thanks the National Research Council of Canada for support and the Department of Materials Science and Engineering at M.I.T. where part of this work was done. The assistance of the Deutsche Forschungsgemeinschaft through a research grant is gratefully acknowledged by A.B. M.A.C. acknowledges the support of the Commonwealth Scientific and Industrial Research Organization.

*Present address: Dépt. de Génie Physique, Ecole Polytechnique, Univ. de Montréal, Montréal, Québec H3C 3A7 Canada.

†Present address: Lehrstuhl für theoretische Chemie, Technische Univ. Munich, D-8046 Garching, West Germany.

‡Present address: Research School of Chem., Australian National Univ., Canberra 2600, Australia.

[1]M. A. Collins, A. Blumen, J. F. Currie, and John Ross, Phys. Rev. B 19, 3630 (1979) (preceding paper).

[2]R. Blinc and B. Žekš, *Soft Modes in Ferroelectrics and Antiferroelectrics,* (North-Holland, Amsterdam, 1974).

[3]J. F. Scott, Rev. Mod. Phys 46, 83 (1974).

[4]W. Cochran, Adv. Phys. 9, 387 (1960); 10, 401 (1961); 18, 157 (1969).

[5]L. D. Landau and E. M. Lifshiftz, *Electrodynamics of Continuous Media* (Pergamon, New York, 1960).

[6]L. E. Cross, ed. *Phase Transitions* (Pergamon, New York, 1973).

[7]L. L. Hench and D. B. Dove, eds., *Physics of Electronic Ceramics* (Dekker, New York, 1972) Secs. A and B.

[8]S. E. Cummins and T. E. Luke, Proc. IEEE 61, 1039 (1973).

[9]H. H. Wieder, J. Appl. Phys. 31, 180 (1960).

[10]E. Fatuzzo, Phys. Rev. 127, 1999 (1962); see also J. C. Burfoot, *Ferroelectrics* (Van Nostrand, London, 1967), p. 218; R. C. Miller and G. Weinreich, Phys. Rev. 117, 1460 (1960).

[11]J. Gonzalez-Ibeas, J. Appl. Phys. 38, 5141 (1967).

[12]T. V. Panchenko, M. D. Volnyanskii, V. G. Monya, and V. M. Duda, Sov. Phys. Solid State 19, 1311 (1977).

[13]V. P. Bender and V. M. Fridkin, Sov. Phys. Solid State 13, 501 (1971).

[14]E. Fatuzzo and W. J. Merz, *Ferroelectricity* (North-Holland, Amsterdam, 1967).

[15]C. Kittel, *Introduction to Solid State Physics,* 4th ed. (Wiley, New York, 1971).

[16]R. A. Cowley, J. D. Axe, and M. Iizumi, Phys. Rev. Lett. 36, 806 (1976).

[17]K. H. Germann, Phys. Status Solidi A 38, K81 (1976).

[18]Y. Iwata, N. Koyano, and I. Shibuya, J. Phys. Soc. Jpn. 35, 1269 (1973).

[19]K. Itoh, H. Matsunaga, and E. Nakamura, J. Phys. Soc. Jpn. 41, 1679 (1976).

[20]M. Balkanski, M. K. Teng, S. M. Shapiro, and M. K. Ziolkiewicz, Phys. Status Solidi B 44, 355 (1971).

[21]P. A. Fleury and K. B. Lyons, Phys. Rev. Lett. 37, 1088 (1976).

[22]H. Iwasaki, K. Sugii, T. Yamada, and N. Niizeki, Appl. Phys. Lett. 18, 444 (1971).

[23]Y. Iwata, H. Koizumi, N. Koyano, I. Shibuya, and N. Niizeki, J. Phys. Soc. Jpn. 35, 314 (1973).

[24]M. I. Kay, R. E. Newnham, and R. W. Wolfe, Ferroelectrics 9, 1 (1975).

[25]S. Nanamatsu, H. Sugiyama, K. Doi, and Y. Kondo, J. Phys. Soc. Jpn. 31, 616 (1971).

[26]J. F. Ryan and K. Hisano, J. Phys. C 6, 566 (1973).

[27]D. Berlincourt, H. Jaffe, W. J. Merz, and R. Nitzsche, Appl. Phys. Lett. 4, 61 (1964).

[28]Y. Iwata, N. Koyano and I. Shibuya, J. Phys. Soc. Jpn. 20, 875 (1965).

[29]Y. Iwata, S. Fukui, N. Koyano, and I. Shibuya, J. Phys. Soc. Jpn. 21, 1846 (1966).

[30]A. Kikuchi, Y. Oka, and E. Sawaguchi, J. Phys. Soc. Jpn. 23, 337 (1967).

[31]E. Fatuzzo, G. Harbeke, W. J. Merz, R. Nitzsche, H. Roetschi and W. Ruppel, Phys. Rev. 127, 2036 (1962).

[32]C. H. Perry and D. K. Agrawal, Solid State Commun. 8, 225 (1970).

[33]P. S. Peercy, Ferroelectrics 16, 193 (1977).
[34]S. M. Shapiro, J. D. Axe, G. Shirane, and T. Riste, Phys. Rev. B 6, 4332 (1972).
[35]T. Riste, ed., *Anharmonic Lattices, Structural Transitions and Melting,* (Noordhoff, Leiden, 1974).
[36]E. P. Maĭshchik, B. A. Strukov, E. V. Sinyakov, K. A. Minaeva, and V. G. Monya, Sov. Phys. Solid State 19, 193 (1977).
[37]J. P. Pouget, S. M. Shapiro, and K. Nassau, BNL-24446 (unpublished).
[38]E. F. Steigmeier, H. Auderset, and G. Harbeke, Phys. Status Solidi B 70, 705 (1975).
[39]A. Pierrefeu, E. F. Steigmeier, and B. Dorner, Phys. Status Solidi B 80, 167 (1977).